Novel View Synthesis using Feature-preserving Depth Map Resampling

Duo Chen, Jie Feng and Bingfeng Zhou
Institute of Computer Science and Technology, Peking University, Beijing, China

Keywords: Novel View Synthesis, Depth Map, Importance Sampling, Image Projection.

Abstract: In this paper, we present a new method for synthesizing images of a 3D scene at novel viewpoints, based on a set of reference images taken in a casual manner. With such an image set as input, our method first reconstruct a sparse 3D point cloud of the scene, and then it is projected to each reference image to get a set of depth points. Afterwards, an improved error-diffusion sampling method is utilized to generate a sampling point set in each reference image, which includes the depth points and preserves the image features well. Therefore the image can be triangulated on the basis of the sampling point set. Then, we propose a distance metric based on Euclidean distance, color similarity and boundary distribution to propagate depth information from the depth points to the rest of sampling points, and hence a dense depth map can be generated by interpolation in the triangle mesh. Given a desired viewpoint, several closest reference viewpoints are selected, and their colored depth maps are projected to the novel view. Finally, multiple projected images are merged to fill the holes caused by occusion, and result in a complete novel view. Experimental results demonstrate that our method can achieve high quality results for outdoor scenes that contain challenging objects.

1 INTRODUCTION

Given a set of reference images of a scene, novel view synthesis (NVS) methods aim to render the scene at novel viewpoints. NVS is an important task in computer vision and graphics, and is useful in areas such as stereo display and virtual reality. Its applications include 3DTV, Google Street View (Anguelov et al., 2010), scene roaming and teleconferencing.

NVS methods can be divided into two categories: *small-baseline* methods and *large-baseline* methods, where "baseline" refers to the translation and rotation between adjacent viewpoints.

In the case of small-baseline problems, some methods focus on parameterizing the plenoptic function with high sampling density. They arrange the camera positions in well-designed manners and sample the scene uniformly with reference images. Typical examples include light field (Levoy et al., 1996) and unstructured lumigraphs (Buehler et al., 2001). Some other methods (Mahajan et al., 2009; Eversen and Koch, 2003) were proposed to produce novel views by interpolating video frames, where adjacent video frames have close viewpoints. Some methods based on optical flow also belong to the small-baseline category.

On the other hand, large-baseline NVS is a challenging, under constrained problem due to the lack of full 3D knowledge, scale changes and complex occlusions. It is thus necessary to seek additional depth and geometry information or constraints like photo-consistency and color-consistency.

For example, Google Street View (Anguelov et al., 2010) directly acquire depth information with laser scanners to interpolate large-baseline images. Some other methods utilize structure-from-motion (SFM) and multi-view stereo (MVS) to recover sparse 3D point cloud of the scene and synthesis novel views based on them. For instance, the rendering algorithm of Chaurasia et al. (Chaurasia et al., 2013) synthesized depth for the poorly constructed regions of MVS and provides a plausible image-based navigation. However, their approach is limited by the capabilities of the oversegmentation, and the very thin structures in the novel view may be missing.

Recent works also address the problem of large-baseline NVS by training neural networks in an end-to-end manner (Flynn et al., 2016). These methods only require sets of posed images as training dataset, and are general since they can give good results on test sets that are considerably different from the training set. These methods are usually slower than MVS based methods, and detailed textures in the images are usually blurred. Moreover, the relationship between 3D objects and their 2D projections has a clear formulation, and requiring neural networks to learn this

Chen, D., Feng, J. and Zhou, B.
Novel View Synthesis using Feature-preserving Depth Map Resampling.
DOI: 10.5220/0007308701930200
In *Proceedings of the 14th International Joint Conference on Computer Vision, Imaging and Computer Graphics Theory and Applications (VISIGRAPP 2019)*, pages 193-200
ISBN: 978-989-758-354-4

relationship is inefficient.

The input of our method is a set of photographs of the scene captured with common commercial cameras, and the camera positions are selected in a casual manner rather than pre-designed. The position of novel viewpoints can also be arbitrary, as long as it is not too far from the existing camera positions. We first reconstruct the scene using SfM and MVS, and the resulting 3D point cloud is projected to reference camera positions to get per-view coarse depth maps. We then apply a feature-preserving sampling and triangulation method to the input images, followed by a depth propagation step to generate dense depth maps. Finally, the novel view can be rendered by an image projection and merging step.

The main contributions of this paper include:

1. We present a method to achieve high quality large-baseline NVS for challenging scenes. The proposed approach decomposes the problem into four steps: 1) sparse 3D point cloud reconstruction, 2) importance sampling, 3) depth propagation and 4)image projection and merging.
2. A novel depth propagation algorithm to generate pixel-wise depth map for reference images based on resampling and triangulation.

2 RELATED WORK

2.1 Image-based Rendering

Unlike traditional approaches based on geometry primitives, image-based rendering (IBR) techniques render novel views based on input image sets. IBR techniques can be classified into different categories according to how much geometry information they use.

Light field rendering (Levoy et al., 1996) and unstructured lumigraphs (Buehler et al., 2001) are representative techniques for rendering with no geometry. They characterize subsets of the plenoptic function from high-density discrete samples, and novel views can be rendered in real time using light fields or lumigraphs. The main limitation of these methods is that they all require high sampling density, and rendering novel views far from the existing viewpoints is very challenging.

View interpolation approaches (Stich et al., 2008; Mahajan et al., 2009) rely on implicit geometry and are able to create high-quality transitions between image sequences or video frames. However, these methods are only suitable for small-baseline tasks and hence beyond our consideration.

Some recent works take advantage of the modern multi-view stereo (MVS) techniques. They utilize the sparse point cloud generated by MVS as geometric proxies, and project input images to the novel view. Since these point clouds usually have poorly constructed regions, Goesele et al. use ambient point cloud (Goesele et al., 2010) to represent unconstructed regions of the scene, and render them in a non-photorealistic style.

2.2 3D Reconstruction

Structure-from-motion (SfM) has been widely used for 3D reconstruction from uncontrolled photo collections. Taken a set of images along with their intrinsic camera parameters as input, a typical SfM system extracts feature points in each image and matches them between image pairs. Then, starting from an initial two-view reconstruction, the 3D point cloud and per image external camera matrix is reconstructed by iteratively adding new images, triangulating feature point matches and bundle-adjusting the 3D points and camera poses (Wu, 2013).

Multi-view stereo (MVS) algorithms can reconstruct reasonable point clouds from multiple photographs or video clips. The method proposed by Furukawa and Ponce (Furukawa and Ponce, 2010) takes multiple calibrated photographs as input, and match images at both per-pixel and per-view level. The matching results are improved by optimizing the surface normal within a photo-consistency measure, and lead to a dense set of patches covering the surfaces of the object or scene.

However, point clouds reconstructed by MVS are still relatively sparse, and their distribution is usually irregular. Although these MVS methods work well for regular scenes like buildings and sculptures, objects with complex occlusions or texture-poor surfaces are usually poorly constructed or totally missing, due to the lack of photo-consistency in these regions. Without accurate depth information, MVS-based NVS approaches are prone to generate unrealistic results, including tearing of occlusion boundaries, elimination of complete textures or aliasing in such challenging scenes.

2.3 Depth Synthesis

When depth information is available for every pixel in reference images, a novel view can be rendered at any nearby viewpoint by projecting the pixels of the reference images back to the 3D world coordinate system and re-projecting them to the novel viewpoint. Thus, synthesizing dense depth maps from sparse ones is

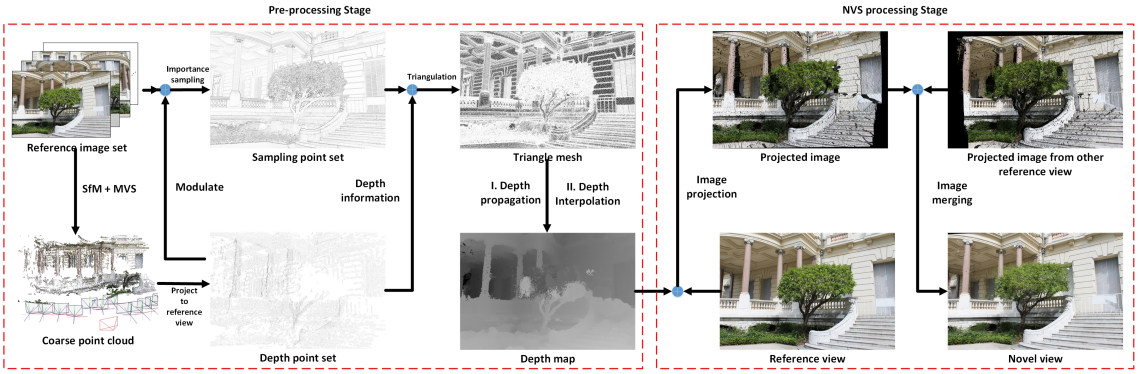

Figure 1: The pipeline of our method.

necessary for our task.

Several works focus on generating dense depth maps by propagating depth samples to the unconstructed pixels of the image. The method proposed by Lhuillier and Quan (Lhuillier and Quan, 2003) reconstructs per-view depth maps and introduce a consistent triangulation of depth maps for pairs of views. Snavely et al. (Snavely et al., 2006) detect intensity edges using a Canny edge detector, and smoothly interpolate depth maps by placing depth discontinuities across the edges. Hawe et al. (Hawe et al., 2011) present an algorithm for dense disparity map reconstruction from sparse yet reliable disparity measurements. They perform the reconstruction by making use of the sparsity in wavelet domain based on the theory of compressive sensing. In the work of Chaurasia et al. (Chaurasia et al., 2013), depth information is synthesized for poorly reconstructed regions based on oversegmented superpixels and a graph traversal algorithm. A following shape-preserving warp algorithm is implemented to achieve image-based navigation.

2.4 Importance Sampling

In this paper, sampling refers to the process of generating a set of representative pixels from continuous images, with certain functions controlling the sampling density in different regions. The sampling point set should preserve the features of input images and has good distribution property.

In 2001, Ostromoukhov proposed an improved error-diffusion algorithm by applying variable coefficients for different key levels (Ostromoukhov, 2001). Zhou and Fang (Zhou and Fang, 2003) made furhter improvement using threshold modulation to remove visual artifacts in the variable-coefficient error-diffusion algorithm. By controlling the level of the modulation strength, an optimal result with blue-noise property can be achieved.

Zhao et al. (Zhao et al., 2013) proposed a high-efficiency image vectorization method based on importance sampling and triangulation. In this method, a sampling point set is generated on the image plane according to an important function defined by structure and color features. Hence this sampling point set can preserve both edge and internal features in the image, and possesses good distribution property. The areas with significant features have higher importance value together with sample point density, and vise verse. By triangulating the sampling points and interpolating color inside the triangles, the image can be easily recovered.

3 OUR APPROACH

3.1 Overview

In this paper, we propose a NVS method based on feature-preserving depth map resampling and triangulation. The input of our method is a set of reference images taken from different viewpoints of a scene (noted as *reference image set*). For a desired novel viewpoint, our method is able to generate plausible novel view image. As shown in Fig.1, the method includes the following steps:

1) 3D reconstruction and Propagation. First, we use SfM to extract camera matrices for each input image and reconstruct a very sparse 3D point cloud of the scene, and then refine it by MVS. The resulting point cloud is projected to each reference viewpoint, providing depth information to a set of points (noted as *depth point set*) in each reference image.

2) Importance Sampling. Next, an importance function is defined based on the boundaries and feature lines in each reference image. Then a *sampling point set* is generated according to the importance function and the depth point set, using an improved error-diffusion algorithm. The sampling points are triangulated to form a triangle mesh.

3) Depth Propation. Afterwards, with a distance metric which considers Euclidean distance, color similarity and color gradient, depth information is propagated from the depth point set to the whole sampling point set, and depth values are interpolated in each triangle to reconstruct a dense depth map.

4) Image Projection and Merging. Finally, given a desired novel viewpoint, several input images are chosen as reference, and their corresponding colored depth maps are projected onto the novel image plane. The projected images are merged, and the holes caused by occlusion are filled to obtain the final image.

Note that in this pipeline, step 1)∼3) belong to the pre-processing stage, and hence runs offline only once. Step 4) is performed online, according to the desired novel viewpoint.

3.2 3D Reconstruction and Projection

Our input is a set of images $\{I_i|i = 1...n\}$ of a 3D scene taken by commercial cameras at different viewpoints, together with their intrinsic matrices $\{K_i|i = 1...n\}$. The camera positions are chosen in a casual manner rather than requiring specific constraints (Fig.2(b)). Instead of reconstructing the complete 3D geometry of the scene, we demonstrate that a sparse point cloud generated by MVS can provide enough depth information to generate reliable pixel-wise depth maps for novel view synthesis.

First, we adopt an SfM method (Wu, 2013) to extract extrinsic matrices for each camera position, that is, $\{R_i|i = 1...n\}$ for rotation and $\{t_i|i = 1...n\}$ for translation. SfM methods can also reconstruct a sparse point cloud of the scene. On the basis of that, we further utilize an MVS method (Furukawa and Ponce, 2010) to refine the 3D point cloud. For the datasets we use in this paper, the MVS method typically reconstruct 100k∼200k points from 10 to 30 images with 4M∼6M resolution. The reconstructed point cloud is irregular for all scenes, regions like vegetation and walls are often poorly reconstructed (Fig.2(c)). The depth information for these regions will be compensated in the following depth synthesis step.

Then, the 3D point cloud is projected to each reference viewpoint, producing a set of projected points with depth information in each input image (Fig.2(c)). The 3D points and their projections are denoted in homogeneous notations $\boldsymbol{P} = (x,y,z,1)$ and $\boldsymbol{p} = (u,v,1)$ respectively. The projection is formulated as:

$$z\boldsymbol{p} = \boldsymbol{K}[\boldsymbol{R}|\boldsymbol{T}]\boldsymbol{P}. \quad (1)$$

Notice that, some of the projected points should be discarded because of occlusions. While the distant objects are usually occulded by the near objects, points belonging to distant objects are hardly occluded by the near points since they are very sparse, and therefore wrong depth values will be introduced to the image.

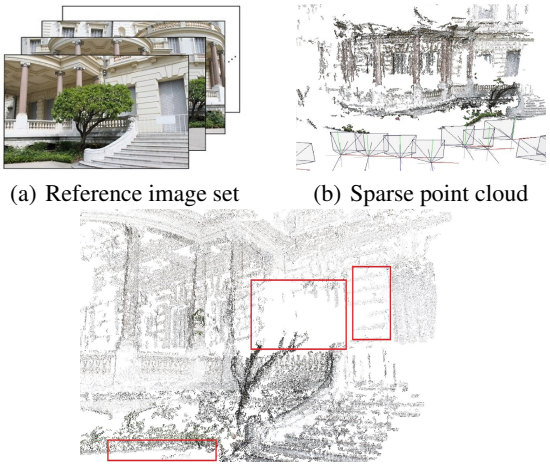

(a) Reference image set (b) Sparse point cloud

(c) Depth point set projected to a reference view

Figure 2: Input images and reconstructed sparse point cloud. Note the poorly reconstructed regions shown in (c).

We tackle this problem by making use of photo-consistency, i.e., a 3D point $P_1 = (r_1,g_1,b_1)$ should have similar color with its corresponding projected point $P_2 = (r_2,g_2,b_2)$ for any viewpoint. Therefore, the projected points whose colors are seriously different from their sources will be marked as outliers and then discarded.

This process also helps to eliminate mistakes in the sparse point cloud. When the global illumination does not change radically, the normal Euclidean distance in the RGB or a modified HSV space works nearly equally for evaluating color changes (Hill et al., 1997). Therefore, the color similarity is measured with the Euclidean distance in RGB color space throughout this paper.

3.3 Importance Sampling

The depth information produced by SfM / MVS techniques is not sufficient for NVS, for significant regions with very sparse or no depth information often exist. That is because MVS methods reconstruct 3D points based on feature points matching and photo-consistency, which will become highly ambiguous for objects with no or repetitive textures and complex geometry like self-occlusions. Besides, the number of reconstructed 3D points is usually less than 5% of the image pixels, hence the projected points will be sparse

-1	-2	-1
0	0	0
1	2	1

-1	0	1
-2	0	2
-1	0	1

2	1	0
1	0	-1
0	-1	-2

0	1	2
-1	0	1
-2	-1	0

Figure 3: The four templates of the improved Sobel operator.

and irregular in the depth maps. Directly interpolating the projected points is prone to create bulky depth maps with errors near object silhouettes.

In general, depth maps usually consist of large smooth regions with homogeneous depth values inside, and between them existing discontinuities where depth values change rapidly. Regarding the work of (Zhao et al., 2013), the large smooth regions can be represented by a small number of sampling points, while a large number of sampling points are needed near the discontinuities.

Although the distribution of smooth regions and discontinuities in depth maps is previously unknown, an assumption can be made that discontinuities in the depth map coincide with the edges in the corresponding reference image. The assumption is not a precise one, but work well even for the datasets with quite complex geometry, and the following processes of sampling and triangulation are robust.

Based on that assumption, we first apply an improved Sobel operator (Fig.3) to the reference images to detect edge features. The improved Sobel operator contains two more template for diagonal lines, hence it is able to detect more detailed and accurate features (shown in Fig.4(a)). Since the resulting gradient values x are integers ranging from 0 to the maxium gradient over the whole image, we define an importance function F to map x from [0,max] to [0,255]:

$$F(x) = 255[1 - (\frac{x}{max})^{\gamma}], x \in [0, max]. \quad (2)$$

Here, $\gamma \in [0,1]$ is a constant that controls the importance function. Higher γ will raise the importance of pixels near the edges, which leads to higher sampling density in these areas, and much lower density in smooth regions. The distribution of sampling points will be more uniform with lower γ. In our implementation, we set γ to 0.8 to achieve high quality NVS. Additionally, the importance values of projected depth points are set to 0 (the highest importance) to make sure they are sampled.

(a) Egde features

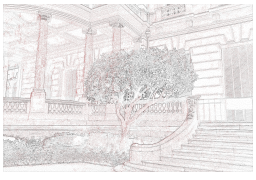

(b) The sampling point set

Figure 4: The gradient map (a) preserves the edge features the reference image. The red points in (b) stand for the original depth points.

So far, we obtain an pixel-wise importance map with importance values ranging from 0 to 255. Then, an improved error-diffusion sampling method (Zhao et al., 2013) is performed according to the importance map to produce the final sampling point set (shown in Fig.4(b)). The number of sampling points is about 10 to 15 % of the total pixels. They have perfect blue-noise distribution property, and preserve the edge and internal features in reference images.

We denote the sampling point as P_s, which includes the subset of projected depth points P_d. Then, taking P_s as vertices, a triangle mesh is generated by Delaunay triangluation (shown in Fig.5(a)). The gradient and depth values can be stored in each vertex for further depth propagation.

(a) Triangle mesh

(b) Depth map

Figure 5: (a) Triangle mesh generated by Delaunay triangulating the sampling points. (b) The generated pixel-wise depth map.

3.4 Depth Propagation

In this step, we propose an efficient and robust approach to propagate depth information from the projected depth point set P_d to the rest of sampling points $P_s^{'} = P_s$-P_d.

A common observation is that, pixels that are spatially close usually belong to the same object and hence have similar depth values, unless there is discontinuity between them. On another aspect, similar color in large smooth regions also implies similar contents and depth values, while color discontinuities roughly coincide with depth discontinuities.

Thus, we can define a distance function to evaluate the similarity between a pair of pixels, based on both color and spatial proximity. Euclidean distance between points P_1 and P_2 is calculated in both RGB color space and reference image coordinate to describe their similarity. Linear weights k_1 and k_2 are introduce to adjust their influence.

However, in complex outdoor scenes, neighboring pixels in reference image may actually belong to

distinct objects with very different depths, and in some situations these pixels also have close colors. Propagating depth information between these pixels will destroy the desired discontinuities in the depth map. We handle this problem by introducing a penalty term C to limit depth propagation across object boundaries. The penalty term between P_1 and P_2 is computed based on the Sobel gradients stored in the vertices which imply object boundaries in the image. The final form of the distance function is:

$$\mathcal{D}(P_1,P_2) = \{k_1[(r_1-r_2)^2+(g_1-g_2)^2+(b_1-b_2)^2] + k_2[(u_1-u_2)^2+(v_1-v_2)^2]\}^{\frac{1}{2}} + C(P_1,P_2). \quad (3)$$

$$C(P_1,P_2) = \underset{\Gamma}{argmin} \sum_{P_i \in \Gamma} g(P_i). \quad (3)$$

Here Γ represents the set of paths between P_1 and P_2 on the triangle mesh. Since larger gradient values imply edges in the image, we take the minimum sum of the gradients along the paths as the penalty term $C(P_1,P_2)$. The shortest path can be calculated by the Dijkstra shortest path algorithm.

During the closest point searching, a five-dimensional kd-tree is built to achieve higher efficiency. The five dimensions of the kd-nodes include (u,v) in the image coordinate and (r,g,b) color values. The distance between kd-nodes is defined similarly to Eq.3, but without the penalty term. Using the kd-tree, we find the nearest P_d for each $P_s^{'}$, and calculate the final distance using Eq.3. Hence, for each point in $P_s^{'}$, its depth value can be propagated from its closest P_d.

After propagating depth information to all the vertices in the triangle mesh, the depth values can be interpolated inside each triangle by a bilinear interpolation and finally generate a dense pixel-wise depth map (shown in Fig.5(b)).

3.5 Image Projection and Merging

After generating dense depth map for each reference image, a novel view can be interpolated by image projection. Given a desired novel viewpoint, we first select several input images as reference based on their camera positions and poses. Then each selected reference image is projected to the novel viewpoint seperately, exploiting its corresponding depth map (Fig.6).

An intuitive approach for image projection is to project each pixel in the reference image to the novel viewpoint discretely. Pixels on the image plane are back-projected to the world coordinate based on their depth and the camera matrices, and then projected to the novel viewpoint. A z-buffer is introduced to handle the occlusions. Regions with no projected pixels will be marked as cracks and holes. Holes often appear near the occusions, while little cracks may appear everywhere.

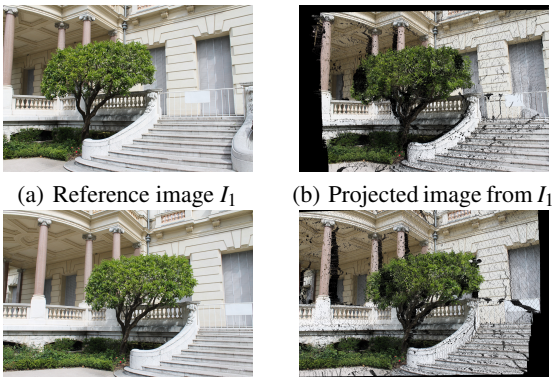

(a) Reference image I_1 (b) Projected image from I_1

(c) Reference image I_2 (d) Projected image from I_2

Figure 6: Projected images from different reference images.

In the final step of our method, all the projected image are merged to form a final result. For each target pixel in the novel view, its source pixels will come from different projected images. Their weights are assigned according to the depth hints and reference camera positions. In general, the projected images whose camera position is closer to the novel viewpoint in terms of spatial and angular proximity will be given higher merging weight. The source pixels may also come from different objects due to occlusions, hence we increase the merging weight of the source pixels with lower depth values. Besides, cracks and holes in the projected image will share no merging weight. After the merging step, the majority of holes and cracks could be filled, and the remaining ones can be further eliminated using median filtering.

4 EXPERIMENTAL RESULTS

We test our NVS method on several datasets from (Chaurasia et al., 2013), including scenes with severe occlusions and challenging objects. In order to evaluate the effectiveness our method, we take one image in each dataset as ground truth and synthesize novel view at the same position. All the algorithms are implemented on a laptop with Intel Core i5-7300 2.50GHz CPU. Note that in our method, all the steps except image projection and merging run only once.

The time costs of all the steps for different datasets and resolution are listed in Table1.

In Fig.7, our synthesizing results are compared to the ground truth. Result images on University and Museum2 datasets are shown in Fig.8 together with corresponding ground truth. In Fig.9 we show the

Table 1: Running time for all the steps.

Dataset	Resolution	Step 1(s)	Step 2(s)	Step 3(s)	Step 4(s)
Museum1	2256*1504	294	78	150	36
Museum1	1200*900	231	27	10	12
Museum2	2256*1504	363	87	103	35
University	1728*1152	168	46	15	19

depth map generated using different set of kd-tree parameters, and demonstrate their effect on the following projection step.

Fig.7 illustrates that our method can produce plausible result image for challenging scenes containing vegetations and complex occlusions. However, neighboring objects with similar color may have very different depth, e.g. white railing in foreground and white window blind in background (lower right in Fig.7(b)). This will lead to misalignment in the depth synthesis step and result in distortions in the result image. Since all the pixels are projected to novel viewpoints discretely, our image projection and merging step cannot ensure the completeness of image texutres. The broken textures will appear as fragments in result image (lower left in Fig.7(b)), and decrease the image quality seriously.

k_1 and k_2 are the two parameters controlling the distance function Eq.3 in triangle mesh, and they stand for the weight of color and spatial proximity respectively. As shown in Fig.9, smaller k_2 leads to bulky depth map, and the object boundaries appear irregular. As the value of k_2 increases, depth map becomes smoother or even be overfitted to the image texture.

Fig.8 demonstrate that our method can render regions with complex texture properly (e.g. words on warning board in Fig.8(b) and the billboard in Fig.8(d)). Objects involving severe occlusion (the huge pillar in Fig.8(b)) can also be well rendered using a simple z-buffer. Besides, the black region on the left edge of Fig.8(b) means that pixels in this area are absent in all other reference images.

(a) Ground truth

(b) Result image

Figure 7: Novel view synthesis result comparison for Museum1 dataset.

5 CONCLUSIONS

In this paper, we propose a novel method for synthesizing novel views from a set of reference images taken in a casual manner. Our method has a pre-processing stage consisting of 3D reconstruciton, importance sampling and depth propagation steps to generate pixel-dense depth maps for each reference view, and a projection and merging step for rendering. We show the efficiency and robusness of our method on some challenging outdoor scenes containing vegetations and complex geometry.

The main limitaion of our method is the rendering speed. We will implement the image projection and merging step on GPU for acceleration, and investigate new rendering algorithms.

Our future work also includes making more use of photo-consistency. Although the sparse point cloud generated by MVS is supposed to be photo-consistent, in some regions of our synthesized depth maps, this desired property will be lost. We would like to refine our depth maps by applying photo-consistency, which will help revising the wrong depth values.

(a) Ground truth (b) Result image

(c) Ground truth (d) Result image

Figure 8: Result comparison for University (a)(b) and Museum2 (c)(d) dataset.

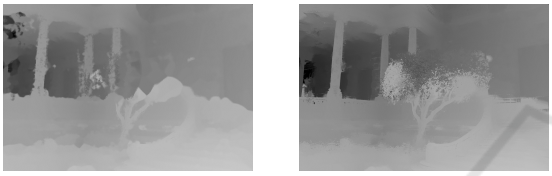

(a) Depth map 1 (b) Depth map 2

Figure 9: Depth maps generated using different kd-tree parameters. (a) the depth map with $k_2 = 0.5\ k_1$, (b) depth map with $k_2 = 10\ k_1$.

ACKNOWLEDGEMENTS

This work was supported by National Natural Science Foundation of China (NSFC) [grant number 61602012].

REFERENCES

Anguelov, D., Dulong, C., Filip, D., Frueh, C., Lafon, S., Lyon, R., Ogale, A., Vincent, L., and Weaver, J. (2010). Google street view: Capturing the world at street level. *Computer*, 43(6):32–38.

Buehler, C., Bosse, M., Mcmillan, L., Gortler, S., and Cohen, M. (2001). Unstructured lumigraph rendering. In *Conference on Computer Graphics and Interactive Techniques*, pages 425–432.

Chaurasia, G., Duchene, S., Sorkine-Hornung, O., and Drettakis, G. (2013). Depth synthesis and local warps for plausible image-based navigation. *Acm Transactions on Graphics*, 32(3):1–12.

Evers-Senne, J. F. and Koch, R. (2003). Image based interactive rendering with view dependent geometry. *Computer Graphics Forum*, 22(3):573582.

Flynn, J., Neulander, I., Philbin, J., and Snavely, N. (2016). Deep stereo: Learning to predict new views from the world's imagery. In *Computer Vision and Pattern Recognition*, pages 5515–5524.

Furukawa, Y. and Ponce, J. (2010). Accurate, dense, and robust multiview stereopsis. *IEEE Transactions on Pattern Analysis and Machine Intelligence*, 32(8):1362–1376.

Goesele, M., Ackermann, J., Fuhrmann, S., Haubold, C., Klowsky, R., Steedly, D., and Szeliski, R. (2010). Ambient point clouds for view interpolation. *Acm Transactions on Graphics*, 29(4):1–6.

Hawe, S., Kleinsteuber, M., and Diepold, K. (2011). Dense disparity maps from sparse disparity measurements. In *International Conference on Computer Vision*, pages 2126–2133.

Hill, B., Roger, T., and Vorhagen, F. W. (1997). Comparative analysis of the quantization of color spaces on the basis of the cielab color-difference formula. *Acm Transactions on Graphics*, 16(2):109–154.

Levoy, Marc, and Hanrahan (1996). Light field rendering. *Computer Graphics*.

Lhuillier, M. and Quan, L. (2003). Image-based rendering by joint view triangulation. *IEEE Transactions on Circuits and Systems for Video Technology*, 13(11):1051–1063.

Mahajan, D., Huang, F. C., Matusik, W., Ramamoorthi, R., and Belhumeur, P. (2009). Moving gradients: a path-based method for plausible image interpolation. In *ACM SIGGRAPH*, page 42.

Ostromoukhov, V. (2001). A simple and efficient error-diffusion algorithm. *Proc Siggraph*, pages 567–572.

Snavely, N., Seitz, S. M., and Szeliski, R. (2006). Photo tourism: Exploring photo collections in 3d. *Acm Transactions on Graphics*, 25(3):pgs. 835–846.

Stich, T., Linz, C., Wallraven, C., Cunningham, D., and Magnor, M. (2008). Perception-motivated interpolation of image sequences. pages 97–106.

Wu, C. (2013). Towards linear-time incremental structure from motion. In *International Conference on 3d Vision*, pages 127–134.

Zhao, J., Feng, J., and Zhou, B. (2013). Image vectorization using blue-noise sampling. *Proceedings of SPIE - The International Society for Optical Engineering*, 8664.

Zhou, B. and Fang, X. (2003). Improving mid-tone quality of variable-coefficient error diffusion using threshold modulation. *Acm Transactions on Graphics*, 22(3):437–444.